INVERSE FLIGHT DYNAMICS AND COMPREHENSIVE ANALYSIS FOR UNSTEADY MANEUVER LOADS PREDICTION

Raghavendra Prasad
Graduate Student
raghavv@iitk.ac.in

Abhishek A.
Assistant Professor
abhish@iitk.ac.in

Department of Aerospace Engineering
Indian Institute of Technology Kanpur, India

ABSTRACT

This paper describes the development of enhanced integration based inverse flight dynamics simulation for helicopters and its application for blade loads prediction using comprehensive analysis for a helicopter undergoing unsteady pull-up maneuver. The existing baseline inverse simulation analysis having rigid blades with only flap degree of freedom, nonlinear blade aerodynamics and dynamic inflow model is refined in two steps: 1) rigid flap only blade model is updated with full coupled rigid flap-lag-torsion equations, and 2) static 2D airfoil table lookup is enhanced by including attached unsteady aerodynamics model. The baseline and refined inverse flight dynamics analysis is used to predict control angles for a 2.1g pull-up maneuver for UH-60A Black Hawk helicopter. The calculated control angles are then used within the university of Maryland Advanced Rotorcraft Code (UMARC2) comprehensive analysis for prediction of blade loads which are compared against the flight test data. The inverse flight dynamics with baseline rotor dynamics is able to predict the correct trend of variation of control angle time history, but peak-to-peak magnitude variation is overpredicted. The peak-to-peak variation shows better correlation with flight test with the addition of unsteady aerodynamics to the inverse simulation. The aerodynamic loads predicted using the calculated controls show similar peak-to-peak magnitudes. However, the pitching moment predictions obtained for only the baseline case of inverse flight dynamics shows all three stall cycles, the other two simulations show only the two retreating blade stalls.

1 INTRODUCTION

The maneuver loads are important for sizing the helicopter rotor, control system, servos and other critical components. The study of unsteady maneuver requires the knowledge of time history of control angles in addition to the aeroelastic analysis. The availability of flight test data in public domain for such a severe maneuver, a dynamic pull-up maneuver that reached 2.12g at 139 knots, for the UH-60A Black Hawk helicopter had facilitated extensive analysis by researchers [1–6] using high-fidelity CFD-CSD as well as Lifting-line based comprehensive analyses. The state-of-the-art CFD/CSD analyses showed fair to good correlation with the flight test data, but were not able to predict advancing blade transonic stall. The mechanism of this transonic stall was first identified in [7] by using the prescribed deformations obtained through measured airloads analysis. It was concluded that the prediction of advancing blade transonic stall (third stall) had strong dependence on the control angles being prescribed for simulating the maneuver. It should be noted that all the studies listed above, prescribed the control and shaft angles measured from the flight test.

For the analyses discussed above, no attempts were made to change rotor control angles to match desired vehicle states. Therefore, inverse flight dynamic analysis is needed, which is the process of calculation of pilot control inputs required to achieve a particular trajectory or maneuver. A detailed discussion of the various inverse simulation procedures currently used for rotorcraft simulations is presented by Thomson and Bradley [8]. Bradley [9,10] and then Hess et al. [11,12] proposed different approaches to solve the helicopter "inverse flight" dynamics problem. While, the method developed by Thomson and Bradley is called "differentiation inverse method" and resembles a "trim" like calculation carried out at every time step. The approach used by Hess et al. is called "integration inverse method" and involves numerical integration, in which, first the entire trajectory for the maneuver is divided into small steps. Then at each instance of time, an estimate of the change in the amplitude of control displacement required to move the aircraft to the next point is carried out. The error in the resulting position is then estimated and an iterative procedure such as Newton-Raphson is used to minimize the error by a series of control displacements. The two approaches have been show to exhibit comparable

accuracy as discussed in [13], the integration method is an order of magnitude slower than the differentiation method, but has become the most widely adopted method, due to its flexibility and the fact that it is independent of the choice of model. The Newton-Raphson step in integration inverse simulation can be replaced by a optimization problem as demonstrated first by de Matteis et al. [14] and then by Celi [15].

It is important to note that most of the inverse simulation analyses either exclude the rotor dynamics or incorporate it in a simplified form. The effort to employ detailed rotor dynamics analysis for inverse simulation has been very few. Rajmohan et al. [16] developed a methodology in which a simplified flight mechanics analysis for a maneuvering helicopter was iteratively coupled to high-fidelity CFD/CSD analysis for the maneuver loads prediction using an approach similar to loose coupling or delta method. Feedback linearization controller was used to track the desired states of maneuver in order to compute the pilot input controls. This methodology showed good convergence of pitch inputs to flight test data for steady flight. The difficulties observed in convergence for maneuvering flight were addressed in Ref. [17] which showed good convergence in both steady and maneuvering flight regimes. These studies focused on the investigation of the numerical convergence issues in the control angle prediction methodology used in inverse simulation with CFD corrected loads. Abhishek and Prasad [18] predicted the variation in controls using integration based inverse flight dynamic analysis using simple rotor dynamics model with linear and nonlinear blade aerodynamics. However, the inverse flight dynamics model used was quite simple and therefore, the focus of the present paper is to study the effect of continued refinement of rotorcraft dynamics model used for inverse simulation and see its impact of overall rotor loads prediction.

In this paper, inverse flight dynamics simulation of UH-60A Black Hawk helicopter is carried out for a dynamic pull-up maneuver using, first, a simple rotor dynamics model with fully articulated rigid blades with hinge offset and having only flap degree of freedom, 2D airfoil table lookup with dynamic rotor inflow. This constitutes the baseline model. The blade dynamics is then refined to rigid coupled flap-lag-torsion system and finally, attached unsteady aerodynamic model is also incorporated to the baseline model to study the effect of fidelity of rotor dynamics model on control prediction capability of inverse simulation algorithm. The derived controls are used as inputs to the refined University of Maryland Advanced Rotorcraft Code (UMARC2) [19] to predict the rotor aerodynamic loads.

2 APPROACH

The analysis is carried out in two steps. First, the inverse flight dynamics analysis is carried out for an unsteady pull-up maneuver using a progressively refined rotor dynamics model. The predicted control angle time history is then used to predict the maneuver loads using UMARC2 comprehensive analysis. The integration inverse simulation method based on the procedure described in [9] is chosen for the inverse simulation, as this procedure is independent of the choice of aerodynamic and structural dynamic models.

2.1 Integration Inverse Method

Integration based inverse flight dynamics simulation approach is chosen for inverse flight dynamics in present study. In this approach vehicle states estimated in body reference frame are first systematically integrated over a constrained time step and then transformed into earth fixed reference frame and compared to the desired vehicle states. The controls are modified by reducing the error between actual and desired states at the end of constrained time step using Newton-Raphson. The main advantage of this procedure is that the inverse flight dynamics model is isolated from the rotor dynamics, which gives the desired flexibility for studying the effect of various modelling refinements. This procedure is explained below.

A dynamic system can be described as a function of states and controls

$$\dot{\mathbf{x}} = f(\mathbf{x}, \mathbf{u}) \tag{1}$$

by using the updated states from the above equation, instantaneous system output can be derived from the following equation, provided that time history of system controls is given.

$$\mathbf{y} = g(\mathbf{x}) \tag{2}$$

But in a situation where time history of desired output is known and sequence of controls that drive the system to achieve the given output are to be determined, system dynamics must be inverted. The basis for inverse simulation can be obtained by differentiating the output equation with respect to time until the required controls appear in the resulting equation.

$$\dot{\mathbf{y}} = \frac{dg}{d\mathbf{x}}\dot{\mathbf{x}} \tag{3}$$

$$\dot{\mathbf{y}} = \frac{dg}{d\mathbf{x}}f(\mathbf{x}, \mathbf{u}) \tag{4}$$

controls can be calculated by inverting the above equation, which takes the form

$$\mathbf{u} = h(\mathbf{x}, \dot{\mathbf{y}}) \qquad (5)$$

thus controls can be written as function of system output and corresponding states.

For the present analysis, the flight dynamics of helicopter is represented by Newton-Euler equations shown below. Though these equations are general for any rigid body, the derivation of external forces X, Y, Z and moments L, M, N, acting along the three body fixed axes of the helicopter, are carried out using a helicopter rotor dynamics model.

Force equilibrium equations

$$m(\dot{u} + qw - rv) + mg\sin\theta = X \qquad (6)$$
$$m(\dot{v} + ru - pw) - mg\sin\phi\cos\theta = Y \qquad (7)$$
$$m(\dot{w} + pv - qu) - mg\cos\phi\cos\theta = Z \qquad (8)$$

Moment equilibrium equations

$$I_{xx}\dot{p} - (I_{yy} - I_{zz})qr + I_{yz}(r^2 - q^2) - I_{xz}(pq + \dot{r}) + I_{xy}(pr - \dot{q}) = L \qquad (9)$$

$$I_{yy}\dot{q} - (I_{zz} - I_{xx})pr + I_{xz}(p^2 - r^2) - I_{xy}(qr + \dot{p}) + I_{yz}(pq - \dot{r}) = M \qquad (10)$$

$$I_{zz}\dot{r} - (I_{xx} - I_{yy})pq + I_{xy}(q^2 - p^2) - I_{yz}(pr + \dot{q}) + I_{xz}(qr - \dot{p}) = N \qquad (11)$$

Kinematics equations

$$p = \dot{\phi} - \dot{\psi}\sin\theta \qquad (12)$$
$$q = \dot{\theta}\cos\phi + \dot{\psi}\sin\phi\cos\theta \qquad (13)$$

where the notations have their usual meaning, e.g. ϕ, θ, and ψ respectively denote the roll, pitch, and yaw attitudes of the helicopter. F_X, F_Y, F_Z are the forces, and L, M, N are the moments acting along the three body fixed axes of the helicopter. It should be noted that the yaw attitude and corresponding yaw rate terms are set to zero for the above set of equations in the present analysis.

Full six degrees of freedom of the vehicle are considered for current analysis: all three translational and rotational degrees of freedom. But it should be noted that the yaw degree of freedom does not play a significant role for the maneuvers being analyzed in this research which primarily involve motion in vertical-longitudinal plane and any out of plane motion is of small magnitude.

In case of a conventional helicopter, the key system states of interest are

$$\mathbf{x} = \{u, v, w, p, q, r\} \qquad (14)$$

and the control inputs that need to be determined are

$$\mathbf{u} = \{\theta_0, \theta_{1c}, \theta_{1s}, \theta_{tr}\}^T \qquad (15)$$

and the desired output $\mathbf{y}$ would be the maneuver trajectory that is to be performed by aircraft.

The simulation is initiated by dividing the entire trajectory for the maneuver into small steps. Then at each instance of time, an estimate of the change in the amplitude of control displacement required to move the aircraft to the next point is carried out. It is assumed that the controls are constant for each time interval $[\mathbf{t}_k, \mathbf{t}_{k+1}]$. Initial guesses of the controls $\mathbf{u}(\mathbf{t}_k)$ are used for the forward simulation. The output $\mathbf{y}(\mathbf{t}_{k+1})$ obtained from the simulation is compared with the desired output $\mathbf{y}^*(\mathbf{t}_{k+1})$. Based on the errors, the guessed controls are modified using, for example, Newton's method. The process repeats itself until the simulation result converges to the desired trajectory at $\mathbf{t}_{k+1}$. Then the analysis is moved to the next time step.

A step by step procedure describing the integration inverse approach is included below:

1. The set of equations of motion is derived.

2. The initial value of the State Vector is calculated.

3. The Desired Trajectory is defined.

4. The trajectory is discretized into Constrained Time Steps.

5. Each constrained time step is further discretized into Elemental Time Steps.

6. The initial guess of the control vector is made by solving the trim problem for initial steady state.

7. The State vector is updated by forward simulation to obtain the actual output at the Constrained Time Step, considering the control vector as constant throughout the entire Constrained Time Step.

8. The deviation of the actual trajectory from the desired trajectory (at Constrained Time Step) is calculated and the Control Vector is updated.

9. The above mentioned steps are repeated until the deviation of the actual trajectory from the desired trajectory reaches a predetermined minute value, which results in the Required Control Vector that is to be applied initially (i.e., at the previous Constrained Step) to achieve approximately desired trajectory at the Constrained Step-1 (i.e., at the new Constrained Step).

10. The above iterative procedure is continued for the remaining constrained steps.

A flowchart describing the implementation of integration inverse simulation procedure to unsteady maneuver is shown in Fig. 1.
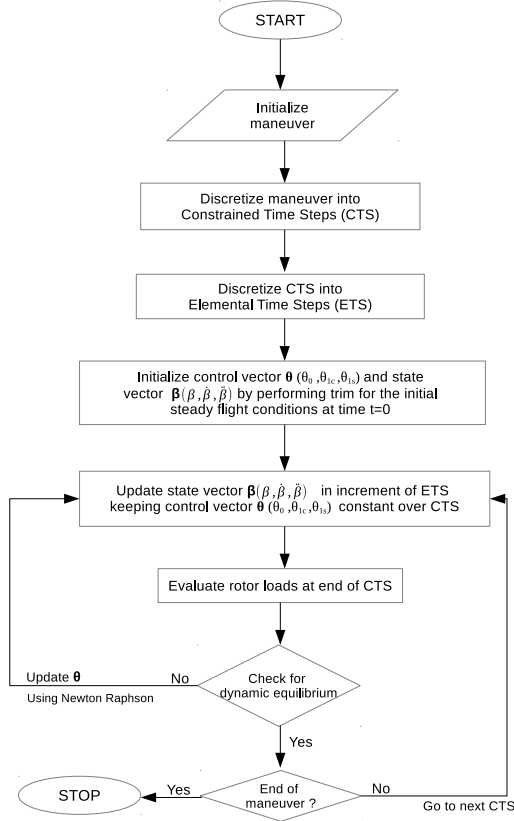
Figure 1: Flow chart depicting integration inverse simulation procedure

2.2 Rotor Dynamics Model for Inverse Simulation

The inverse simulation is carried out using three different rotor dynamics models which are refined progressively.

2.2.1 Baseline Model

The baseline model is the case with the main rotor of the helicopter modeled as fully articulated rotor with rigid blades with hinge offset and having only the flap degree of freedom. Appropriate hinge offset is selected to match the first flap frequency. Rotor blade non-linear aerodynamics are included with the aid of two different airfoil tables corresponding to SC1095 and SC1094R8, which are used for rotor blades of UH-60A Black Hawk helicopter. Since, the lookup tables for the airfoils used on the UH-60A Black Hawk Helicopter is available in public domain, it is used for non-linear quasi-steady aerodynamic calculations during this analysis.The detailed rotor geometry and blade properties data for UH-60A is taken from Refs. [20–23]. Dynamic inflow model developed by Pitt and Peters [24] is incorporated to take

the time lag between inflow and rotor loads, and the effect of forward flight into account. The Pitt-Peters dynamic inflow model for helicopter axial and steady forward flight is formulated as

$$
\begin{bmatrix} M \end{bmatrix} \begin{Bmatrix} \dot{\lambda_0} \\ \dot{\lambda_{1s}} \\ \dot{\lambda_{1c}} \end{Bmatrix} + \begin{bmatrix} V \end{bmatrix} \begin{bmatrix} L \end{bmatrix}^{-1} \begin{Bmatrix} \lambda_0 \\ \lambda_{1s} \\ \lambda_{1c} \end{Bmatrix} = \begin{Bmatrix} C_T \\ -C_L \\ -C_M \end{Bmatrix}
$$
(16)

where λ_0, λ_{1c} and λ_{1s} are the mean induced inflow, longitudinal and lateral inflow gradients across the rotor disk respectively. The apparent mass matrix [M], mass flow parameter matrix [V] and inflow matrix [L], respectively, can be written as

$$
\begin{bmatrix} M \end{bmatrix} = \begin{bmatrix} \frac{128}{75\pi} & 0 & 0 \\ 0 & \frac{16}{45\pi} & 0 \\ 0 & 0 & \frac{16}{45\pi} \end{bmatrix}
$$
(17)

$$
\begin{bmatrix} V \end{bmatrix} = \begin{bmatrix} V_m & 0 & 0 \\ 0 & \bar{V} & 0 \\ 0 & 0 & \bar{V} \end{bmatrix}
$$
(18)

$$
\begin{bmatrix} L \end{bmatrix} = \begin{bmatrix} \frac{1}{2} & 0 & -\frac{15\pi}{64}\chi \\ 0 & 2(1+\chi^2) & 0 \\ \frac{15\pi}{64}\chi & 0 & 2(1-\chi^2) \end{bmatrix}
$$
(19)

where χ (the wake skew angle), the mass flow parameters V_m and $\bar{V}$ associated with mean and higher harmonics of inflow are given as

$$
V_m = \sqrt{\mu^2 + (\lambda_0 + V_c)^2}
$$
$$
\bar{V} = \frac{\mu^2 + (\lambda_0 + V_c)(2\lambda_0 + V_c)}{V_m}
$$
$$
\chi = \arctan\left(\frac{\mu}{\lambda_0 + V_c}\right)
$$

where V_c is climb velocity. System of dynamic inflow equations is solved using Newmark's algorithm.

2.2.2 Case 1

The baseline rigid flap only blade equations are replaced with coupled flap-lag-torsion blade dynamics equations to constitute case 1. In this model, rotor blade is assumed to be rigid and undergoes three degrees of motion: flap, lag and torsion rotations about three hinges [25]. The system of equations for coupled blade deformation can be written as

$$
\begin{bmatrix} 1 & 0 & -I_{*_x} \\ 0 & 1 & 0 \\ -I_{*_x} & 0 & -I_{*_f} \end{bmatrix} \begin{Bmatrix} \overset{**}{\beta} \\ \overset{**}{\zeta} \\ \overset{**}{\theta} \end{Bmatrix} + \begin{bmatrix} 2\frac{\omega_{\beta 0}}{\omega}\zeta_\beta & -2\beta & 0 \\ 2\beta & 2\frac{\omega_{\beta 0}}{\omega}\zeta_L & -2\beta I_{*_x} \\ 0 & 2\beta I_{*_x} & 2\frac{\omega_{\theta 0}}{\omega}\zeta_\theta \end{bmatrix}
$$

$$
\begin{Bmatrix} \overset{*}{\beta} \\ \overset{*}{\zeta} \\ \overset{*}{\theta} \end{Bmatrix} + \begin{bmatrix} v_\beta^2 & 0 & -I_{*_x} \\ 0 & v_\zeta^2 & 0 \\ -I_{*_x} & 0 & -I_{*_f}v_\theta^2 \end{bmatrix} \begin{Bmatrix} \beta \\ \zeta \\ \theta \end{Bmatrix}
$$

$$
= \gamma \begin{Bmatrix} \bar{M}_\beta \\ \bar{M}_\zeta \\ \bar{M}_\theta \end{Bmatrix} + \begin{Bmatrix} \frac{\omega_{\beta 0}^2}{\omega^2}\beta_p \\ 0 \\ I_{*_f}\frac{\omega_{\theta 0}^2}{\omega^2}\theta_{con} \end{Bmatrix}
$$

$$\text{(20)}$$

where β, ζ and θ are flap, lag and torsional deflections of rotor blade. v_β, v_ζ and v_θ are non-dimensional rotating frequencies of flap, lag and torsion respectively. I_{*_x} and I_{*_f} are flap-weighted pitch-flap coupling inertia and pitch inertia respectively. $\omega_{\beta 0}$, $\omega_{\zeta 0}$ and $\omega_{\theta 0}$ are non-rotating flap, lag and torsional frequencies. ζ_β, ζ_L and ζ_θ are viscous damping ratios in flap, lag and torsional modes. θ_{con} is control system command pitch. γ and β_p represent rotor lock number and blade precone angles respectively. The system of rigid flap-lag-torsion equations is solved using Newmark's algorithm.

2.2.3 Case 2

The attached unsteady aerodynamics model, developed by Leishman et al. [26], is further incorporated to the analysis to improve unsteady lift and pitching moment estimation on rotor blades operating under attached-flow conditions in a compressible flow. This refinement is included in the model considered for case 1 and the resulting analysis constitutes case 2.

In this model, the unsteady airloads due to an arbitrary forcing are represented in a state-space form and the unsteady aerodynamic response is described in terms of a two-input/two-output system where the inputs are the airfoil angle of attack and pitch rate and the outputs are the unsteady normal force (lift) and pitching moment. This system is represented in the general form as:

$$\dot{\mathbf{x}} = \mathbf{A}\mathbf{x} + \mathbf{B} \begin{Bmatrix} \alpha \\ q \end{Bmatrix}$$

$$\begin{Bmatrix} C_N \\ C_M \end{Bmatrix} = \mathbf{C}\mathbf{x} + \mathbf{D} \begin{Bmatrix} \alpha \\ q \end{Bmatrix}$$

where the matrices are of the form

$$\mathbf{A} = \mathbf{diag} \begin{bmatrix} a_{11} & a_{22} & a_{33} & a_{44} & a_{55} & a_{66} & a_{77} & a_{88} \end{bmatrix}$$

$$\mathbf{B} = \begin{bmatrix} 1 & 1 & 1 & 0 & 1 & 1 & 0 & 0 \\ 0.5 & 0.5 & 0 & 1 & 0 & 0 & 1 & 1 \end{bmatrix}$$

$$\mathbf{C} = \begin{bmatrix} c_{11} & c_{21} & c_{13} & c_{14} & 0 & 0 & 0 & 0 \\ c_{21} & c_{22} & 0 & 0 & c_{25} & c_{26} & c_{27} & c_{28} \end{bmatrix}$$

$$\mathbf{D} = \begin{bmatrix} \frac{4}{\mathbf{M}} & \frac{1}{\mathbf{M}} \\ \frac{-1}{\mathbf{M}} & \frac{-7}{12\mathbf{M}} \end{bmatrix}$$

The total aerodynamic lift and pitching moment response to an arbitrary time history of α and q can be obtained from the preceding state equations by integrating numerically the system of equations shown above. The various coefficients listed in the equation have their usual meaning and their values have been taken from [26].

In all the cases explained above tail rotor is modeled based on Blade Element Theory (BET) and the tail rotor inflow is calculated using uniform inflow. The side force contribution of the tail rotor is included in the equation of motion to compensate for the main rotor torque required to maintain stable yaw.

The relevant parameters used for helicopter dynamics modeling are shown in Table 1.

Table 1: Helicopter parameters used for inverse simulation

Main Rotor	UH-60A
Number of Blades, N	4
Radius, R (m)	8.17
Blade Chord, c (m)	0.52
Rotational Speed, Ω (rad/s)	27.01
Longitudinal Shaft Tilt (degs.)	-3
Linear Blade Twist, θ_{tw} (rad/m)	-0.3142
Lock Number, γ	6.33
Blade Flap Frequency, v_β	1.04
Fuselage	
Gross Weight (kg)	7876.18
Roll Inertia, I_{xx} (kg-m^2)	4659
Pitch Inertia, I_{yy} (kg-m^2)	38512
Yaw Inertia, I_{zz} (kg-m^2)	36800
Product of Inertia, I_{xz} (kg-m^2)	1882
Tail Rotor	
Number of Blades, N_t	4
Radius, R_t (m)	1.6764
Blade Chord, c_t (m)	0.24
Rotational Speed, Ω_t (rad/s)	124.62
Linear Blade Twist, θ_{tw} (rad/m)	0

2.3 University of Maryland Advanced Rotorcraft code (UMARC2)

As mentioned earlier, the controls time history derived by inverse flight dynamics simulation is fed to

the refined University of Maryland Advanced Rotor-craft Code(UMARC2) to calculate the rotor blade loads. UMARC2 has a structural dynamics model in which the rotor model consists of flexible blades, rigid root end control components and a swashplate model. Each blade is modeled as a fully articulated beam with co-incident flap and lag hinges. The lifting line aerodynamic model is a Weissinger-L type lifting-surface model iteratively coupled to 2D airfoil tables (non-linear near wake), Leishman-Beddoes 2D unsteady aerodynamics [27], and a time accurate transient free wake model based on Ananthan and Leishman [28]. The detailed description of UMARC2 is available in [2, 19].
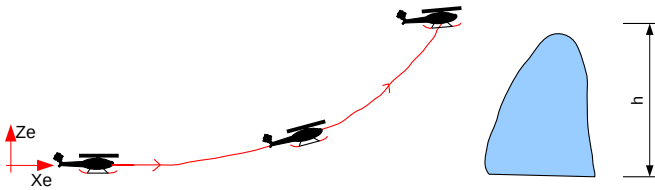
Figure 2: Picture depicting pull-up maneuver
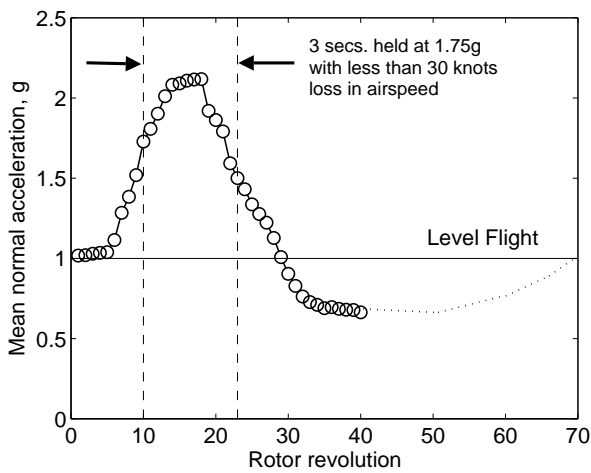
Figure 3: Picture depicting Measured mean load factor for pull-up maneuver

2.4 Maneuver Description

Pull-up maneuver simulated here for UH-60A Black Hawk helicopter is a terrain avoidance maneuver and is initiated from a high speed steady flight by pitching-up the helicopter for a rapid gain in altitude as shown in Fig. 2. Unlike the pop-up maneuver, in which collective is initiated to accelerate vertically, longitudinal shaft tilt is initiated to pitch-up the helicopter that results in an upward tilt in rotor thrust vector resulting in vertical acceleration.
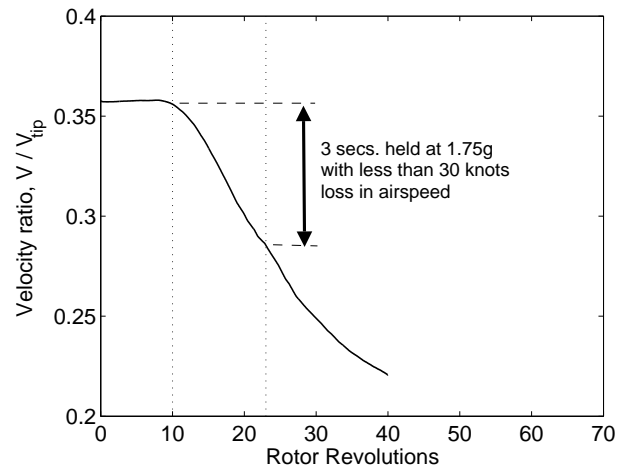
Figure 4: Picture depicting velocity ratio for pull-up maneuver

The maneuver being simulated is the counter 11029 flight from UH-60A flight test database. During this maneuver a maximum load factor of 2.12g was attained. The maneuver lasted for 9 seconds covering 40 rotor revolutions. The flight test data is taken from [1, 2]. The measured load factor and velocity ratio are shown in Figs. 3 and 4. One of the key requirements of this maneuver was to maintain a load factor of 1.75g for 3 seconds with less than 15 m/s loss in airspeed. The helicopter attitude angles and angular rates are shown in Figs. 5 and 6 respectively, with negative representing the nose down attitude. The variation of longitudinal and vertical non-dimensional acceleration of helicopter, for pull-up maneuver, is shown as a function of time in Fig. 7
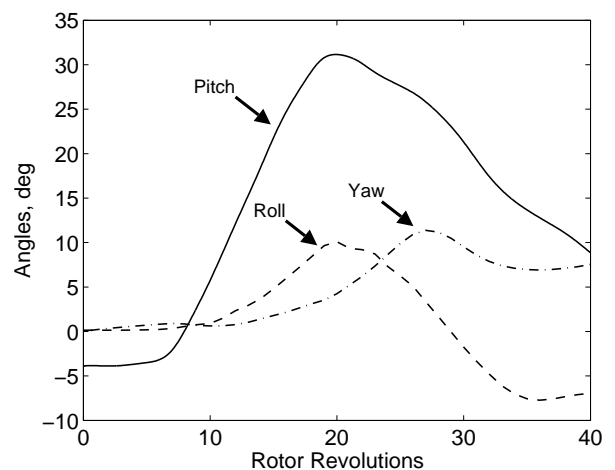

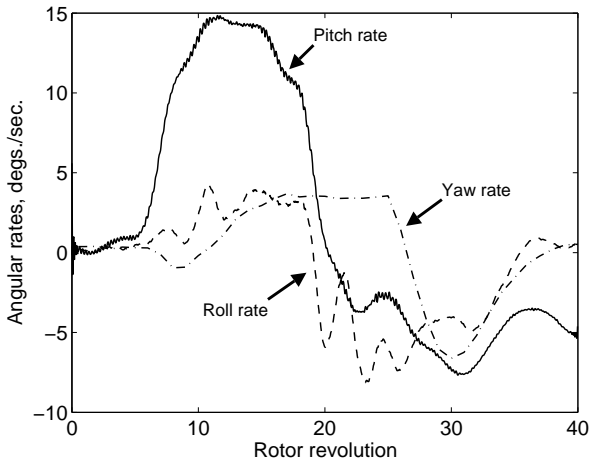Figure 5: Picture depicting helicopter attitude for pull-up maneuver

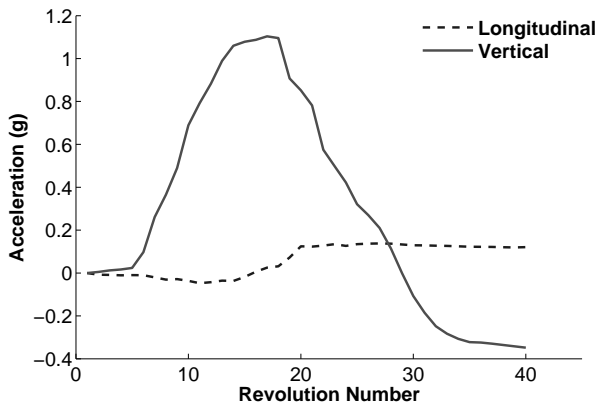Figure 6: Picture depicting helicopter attitude for pull-up maneuver

Figure 7: Variation of acceleration for pull-up maneuver

3 RESULTS

The inverse flight dynamics simulation of the maneuver is carried out using three different rotorcraft models. The control angle time history predicted from the analyses is then used for predicting the blade aerodynamic loads.

3.0.1 Control Angles Predicted Using Inverse Simulation

As mentioned earlier the dynamic pull-up maneuver is simulated for UH-60A helicopter using a baseline rotor dynamics model which has non-linear blade aerodynamics and Pitt-Peter's dynamic inflow model. The predicted controls are compared with the available flight test data to validate the overall methodology. Then the analysis is refined by adding the rigid flap-lag-torsion coupled blade dynamics and unsteady aerodynamics to the rotorcraft dynamics model to understand the effect
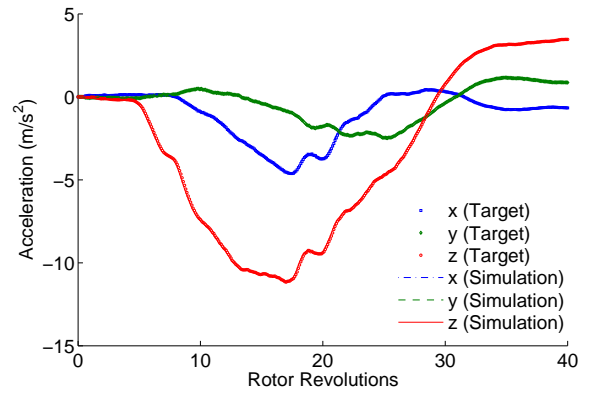
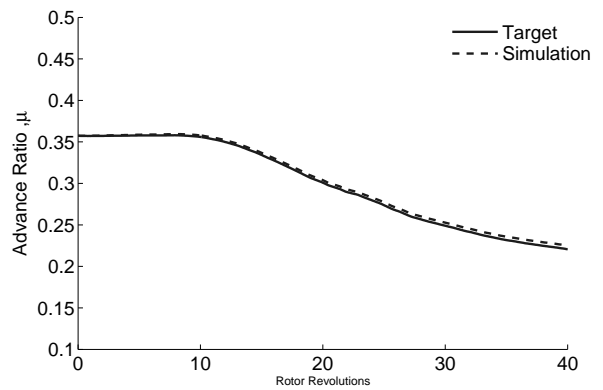Figure 8: Desired and achieved aircraft accelerations in gravity frame

Figure 9: Desired and achieved aircraft velocity in body fixed frame

of each of the refinements on control angle prediction using inverse simulation methodology.

The helicopter's rigid body accelerations in the gravity reference frame are used as the desired vehicle states for the inverse flight dynamics simulation. The time history of desired vehicle accelerations (obtained using flight test linear accelerations and shaft attitudes) are compared to those generated by the inverse simulation analysis in Fig. 8. The algorithm is able to attain the desired vehicle accelerations and maintain it during the entire duration of the maneuver. Since, the vehicle accelerations have been matched so accurately, it is observed that the vehicle is also able to achieve the desired variation in its forward speed during the entire maneuver. Even though the desired vehicle speed is not targeted directly, the time history of desired forward speed compares well with the flight test data and is shown in Fig. 9.

The time history of measured and predicted collective, lateral cyclic and longitudinal cyclic angles, for the baseline, case 1 and case 2, are shown in Figs. 10, 11, and 12 respectively. The flight test collective angle shown in Fig. 10 is observed to remain constant during initial steady flight regime (1–5 revolutions) of the maneuver. The predicted results for all three cases show
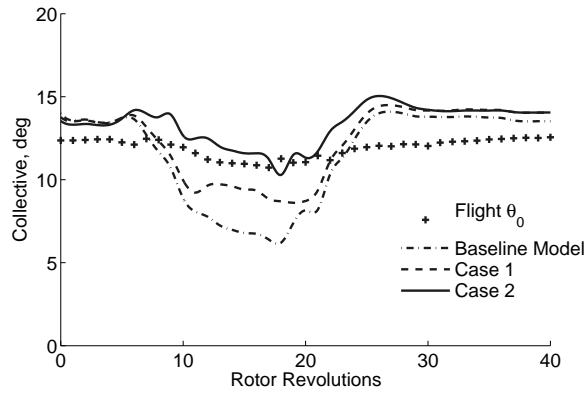
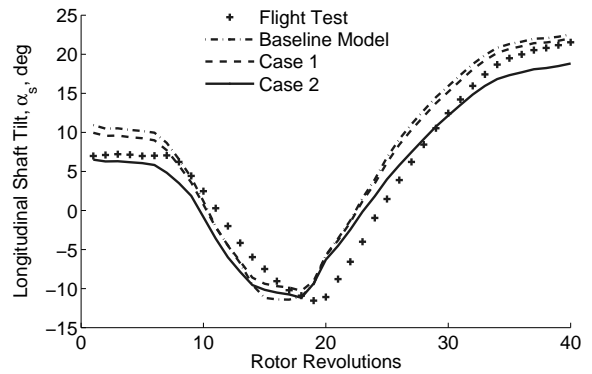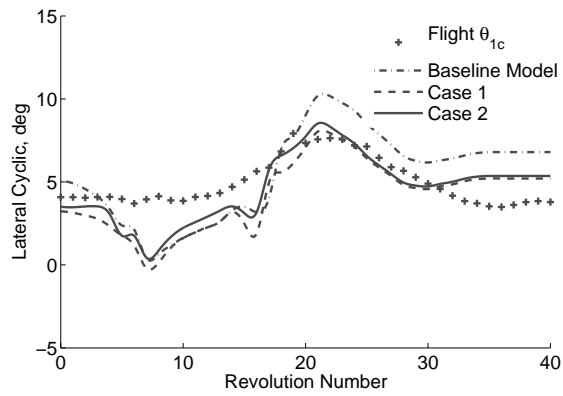Figure 10: Time history of measured and predicted collective pitch angles

Figure 11: Time history of measured and predicted lateral cyclic pitch angles
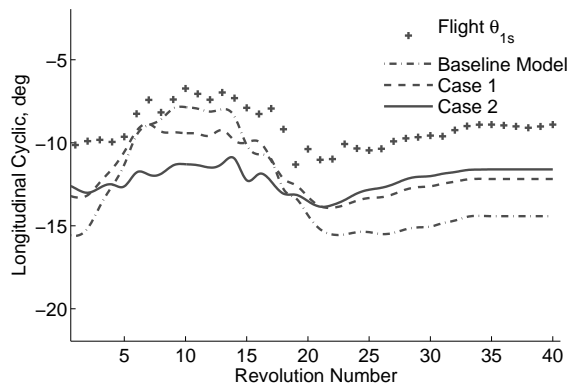

Figure 12: Time history of measured and predicted longitudinal cyclic pitch angle

Figure 13: Time history of measured and predicted longitudinal shaft tilt angles
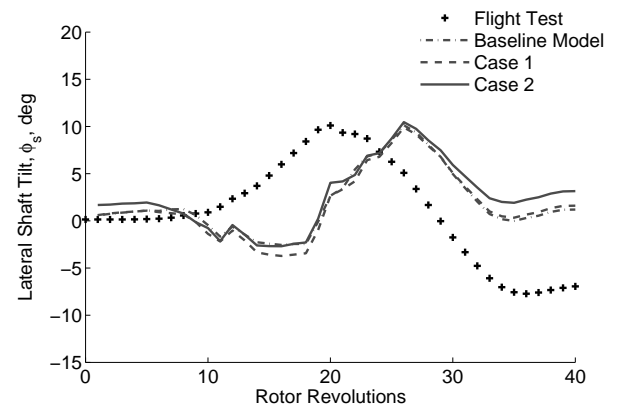

Figure 14: Time history of measured and predicted lateral shaft tilt angle

similar trend during this portion of the maneuver. During the rotor revolution number 10–19, which represents a high velocity and high load factor regime of the maneuver, a significant reduction in required collective is observed despite of the increase in helicopter load factor. This is probably due to the additional inflow at the rotor due to high upward velocity of the helicopter and the analysis is able to predict this trend quite accurately. During revolutions 20–35 a gradual increase in collective control is observed despite reduction in load factor owing to the fact that additional inflow that was available to the rotor is reduced due to decrease in vertical flight velocity. Since helicopter tries to recover to its normal steady flight during last few revolutions (i.e., 32 to 40) of the maneuver, the required collective increases at a gradual rate. The inverse simulation is also able to predict this gradual increase in collective angle beyond revolution 28. The baseline case shows significant overprediction in peak-to-peak collective angle variation, while the case 1 shows relatively less overprediction. Case 2 is showing best peak-to-peak and trend correlation with the flight test data.

The time history of predicted lateral cyclic angles are shown in Fig. 11 and have similar trend as flight test. However, each of the three cases consistently overpredict the peak-to-peak magnitude. It should be noted that the maneuver being analyzed is primarily a longitudinal maneuver and hence the lateral cyclic angle has less influence over the overall vehicle motion. Further, the heading and sideslip angles have not been taken in to account during the inverse simulation analysis, which may result in the differences between the predicted and measured lateral control angle.

Figure 12 shows the time history of longitudinal cyclic for all three cases of the inverse simulation. The overall trend shows excellent correlation for all three flight cases, but the peak-to-peak variation is overpredicted. The extent of overprediction is again reducing from Baseline case to case 2.

The variation of longitudinal shaft angle for all the three cases is shown in Fig. 13. The variation of longitudinal shaft angle predicted by the inverse simulation is in good agreement with the measured flight test data. Again, the results from the case 3 show the best correlation among the three cases considered. The variation of the lateral shaft angle is shown in Fig. 14. None, of the three predictions follow the exact trend observed in the flight test. This may be due to the fact that the sideslip angle which is of significant magnitude in the flight test data has not been included in the inverse simulation analysis.

3.0.2 Blade Loads Predicted Using Comprehensive Analysis

The control time history derived from inverse simulation for UH-60A helicopter to track the path defined by pull-up maneuver is fed to the refined University of Maryland Advanced rotorcraft code (UMARC2) to predict rotor blade loads.

The predicted rotor thrust for the three sets of controls angle time history is shown in Fig. 15. The thrust predicted using measured control data from flight test is also given for reference. Since measured thrust data from flight test is not available it is calculated by multiplying the load factor data with vehicle weight for the present analysis. It can be seen from Fig. 15 that all predictions show good correlation with the flight test data during the entire flight regime. The differences in the prediction and the flight test data are primarily due to the lack of inclusion of the thrust generated by the horizontal stabilizer of the helicopter in the analysis.

The measured and predicted normal force at blade radial station at 86.5% of radius is depicted in Fig. 16. The predictions for mean normal force are in good agreement with the measured normal force for flight test data except the absence of high-frequency loads during high load factor regime of the maneuver. This is because lifting-line based analysis can not predict these stall-dominated high-frequency loads. The slight underprediction of normal force using baseline control angles during the flight regime between rotor revolutions 38–40 can be seen in Fig. 16(d) which is causing the underprediction of rotor thrust observed in Fig. 15. The normal force prediction is less sensitive to the changes in control angle and hence the predicted normal force for all three cases is quite comparable.

The time history of measured and predicted blade pitching moment at 77.5% radial station is shown in Fig. 17. All the three stall cycles were predicted with the control angles obtained with baseline inverse flight dynamics model while the other two cases of simulation predict only two stall cycles on the retreating side of the rotor disk. Negative peak is significantly underpredicted for all the three cases of analysis, but the negative peak of the two stall cycles on the retreating side is relatively better predicted using the control angles from case 2. The prediction of the dynamic stall cycles is known to be sensitive to the overall angle of attack being set by the trim angles and the blade response. The differences observed in the predicted pitching moment is primarily due to the differences in the control angles for the three cases.
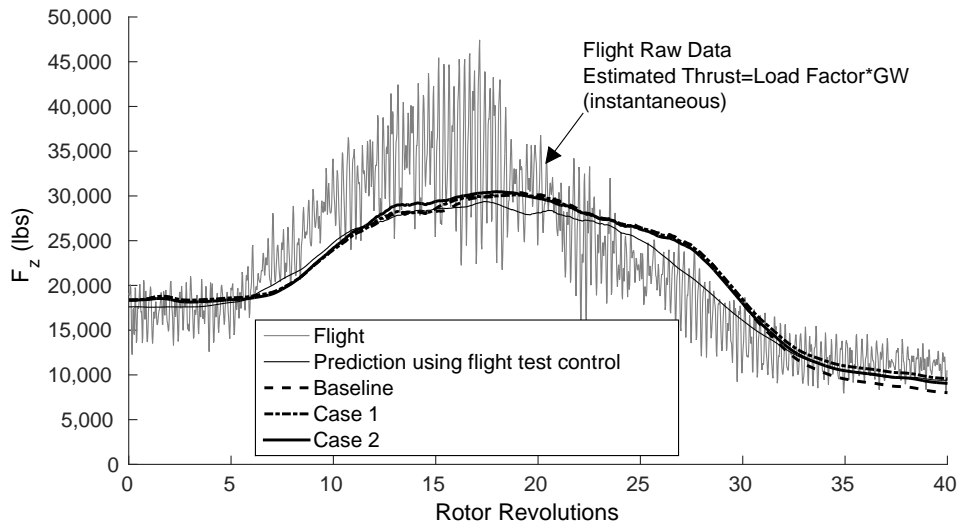
Figure 15: Measured and predicted rotor thrust for C11029 pull-up maneuver; inverse flight dynamics simulation case 1: linear aerodynamics and case 2: non-linear aerodynamics
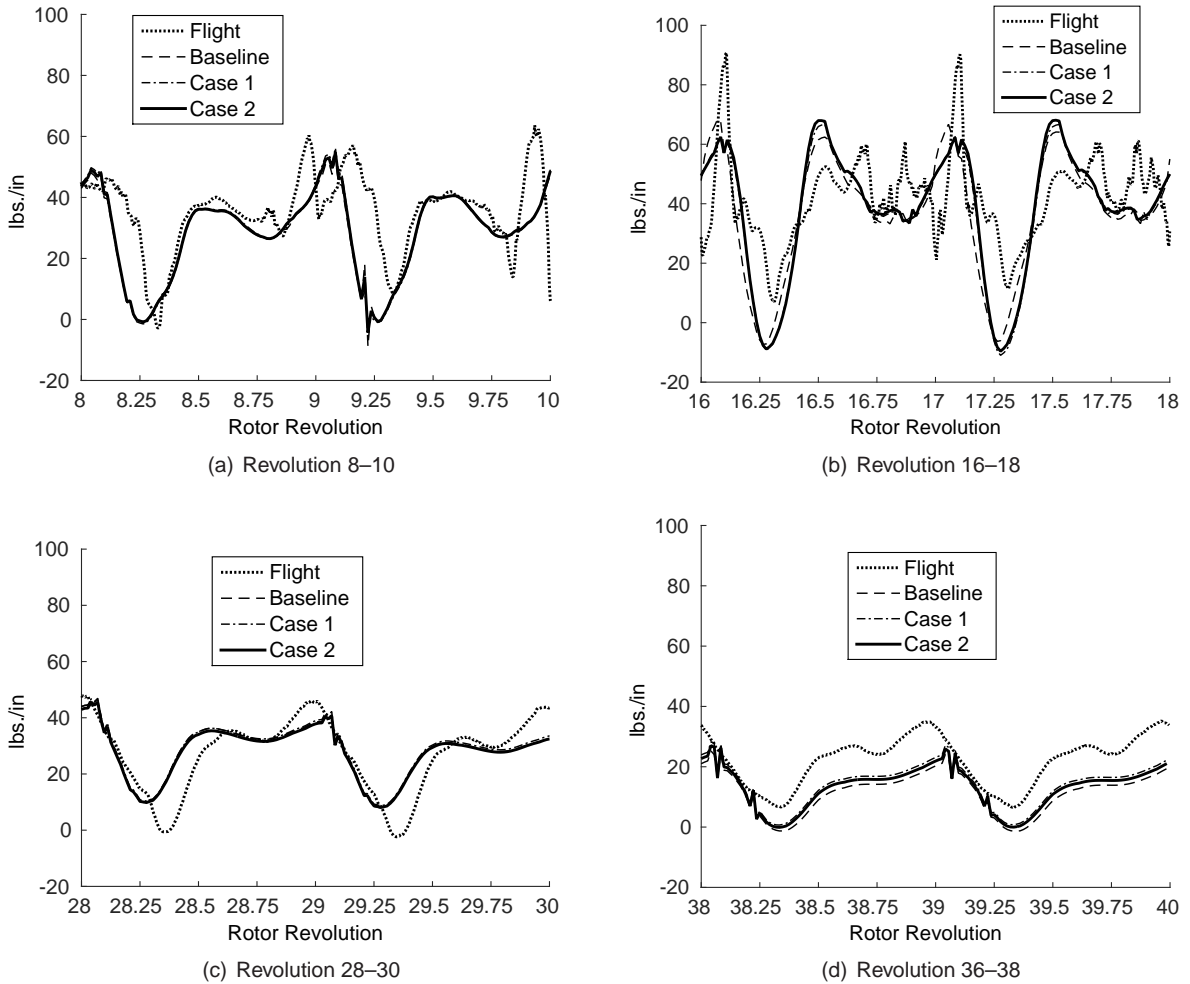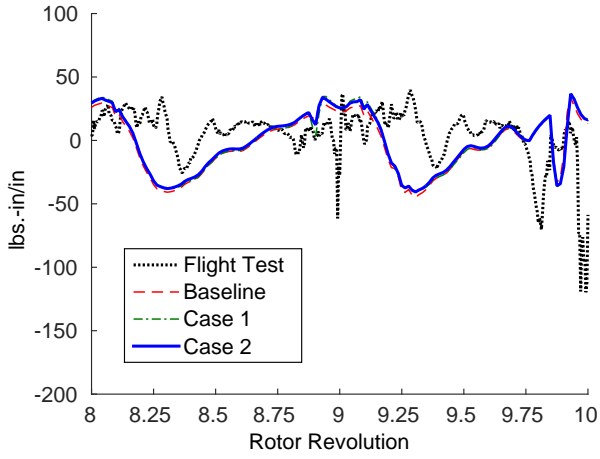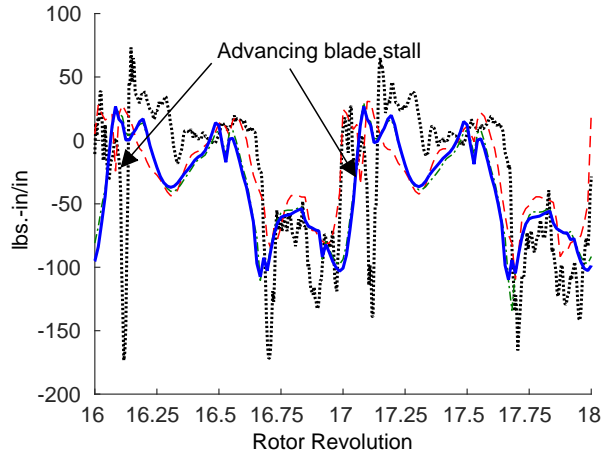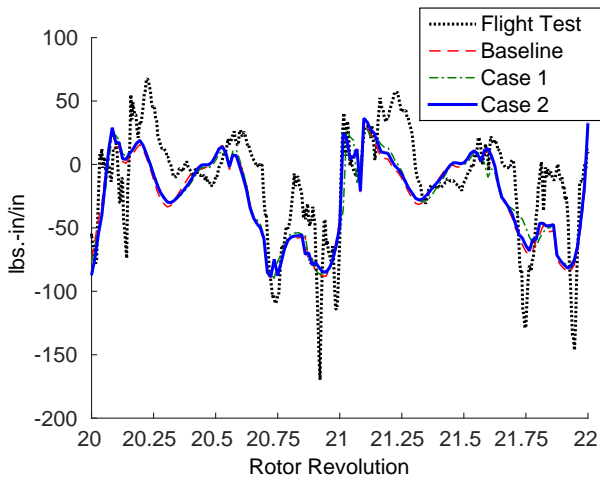

Figure 16: Measured and predicted normal force at 86.5%R for C11029 maneuver; inverse flight dynamics simulation case 1: linear aerodynamics and case 2: non-linear aerodynamics
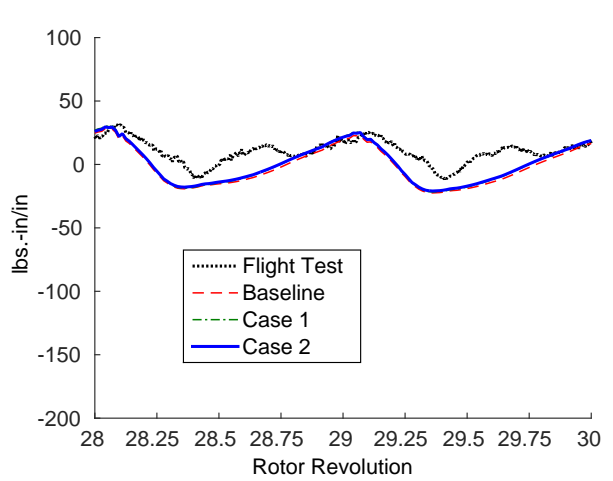
Figure 17: Measured and predicted pitching moment at 77.5%R for C11029 maneuver; inverse flight dynamics simulation case 1: linear aerodynamics and case 2: non-linear aerodynamics

4 SUMMARY & CONCLUSIONS

An integration based inverse flight dynamics simulation algorithm has been developed and the inherent rotorcraft dynamics model used in the inverse simulation is progressively refined to predict the control angles for a 2.1g pull-up maneuver performed by UH-60A helicopter. The effect of changing the fidelity of rotor dynamics is investigated by simulation of the same maneuver using two refined versions of baseline rotor dynamics model (inclusion of flap-lag-torsion coupled blade dynamics and unsteady aerodynamics). The predicted control angles are then used within UMARC2 to predict rotor aerodynamic loads. From this analysis the following key conclusions are drawn:

1. The fidelity of rotor dynamics model has a strong impact on the control prediction capability of inverse flight dynamics simulation algorithm. It is evident from the variation of controls predicted using several refinements to the baseline rotor dynamics model. The time history of collective pitch angle (θ_0) and longitudinal cyclic angle (θ_{1s}) show significantly improved peak-to-peak correlation with flight test data with each successive refinement. The aim is to eventually be able to use the structural dynamics model inherent in the comprehensive analysis for inverse simulation to facilitate improved control angle and loads prediction.

2. The control angle time history predicted by the baseline inverse simulation model when used within UMARC2 enables the prediction of all three stalls, including the advancing blade transonic stall. The enhanced inverse simulation models though show better correlation with flight data, are unable to predict transonic stall. It is known that a correct combination of airfoil control and 5/rev nose-up pitching moment is required for the advancing blade stall prediction. The high peak-to-peak magnitude variation of control angles obtained with baseline inverse simulation may be causing the blade airfoil to achieve the required high angle-of-attack to undergo transonic stall. The right angle of attack may not be getting attained for the remaining two cases.

Acknowledgment

References

[1] Bhagwat, M.J., Ormiston, R.A., Saberi, H.A., and Xin, H., "Application of Computational Fluid Dynamics/Computational Structural Dynamics Coupling for Analysis of Rotorcraft Airloads and Blade Loads in Maneuvering Flight," *Journal of the American Helicopter Society*, Vol. 57, No. 3, July 2012, pp. 1–21.

[2] Abhishek, Datta, A., Ananthan, S., and Chopra, I., "Prediction and Analysis of Main Rotor Blade Loads in a Prescribed Pull-Up Maneuver," *Journal of Aircraft*, Vol. 47, No. 4, July–August 2010, pp. 1197–1215.

[3] Yeo, H., "Investigation of Rotor Airloads and Structural Loads in Maneuvering Flight," American Helicopter Society 64th Annual Forum and Technology Display, Montréal, Canada, April 29–May 1, 2008.

[4] Sitaraman, J., and Roget, B., "Prediction of Helicopter Maneuver Loads Using a Fluid–Structure Analysis," *Journal of Aircraft*, Vol. 46, No. 5, September 2009, pp. 1770–1784.

[5] Thomas, S., Shreyas, A., and Baeder, J., "Wake coupling CFD-CSD Analysis of helicopter rotors in steady and maneuvering flight conditions," American Helicopter Society Aeromechanics Specialists Conference, San Francisco, CA, January 20–22, 2010.

[6] Silbaugh, B., and Baeder, J., "Coupled CFD/CSD Analysis of a Maneuvering Rotor Using Staggered & Time-Accurate Coupling Schemes," AHS Specialist's Conference on Aeromechanics, San Francisco, CA, January 23–25, 2008.

[7] Abhishek, Ananthan, S., Baeder, J., and Chopra, I., "Prediction and Fundamental Understanding of Stall Loads in UH-60A Pull-up Maneuver," *Journal of the American Helicopter Society*, Vol. 56, No. 4, October 2011.

[8] Thomson, D.G., and Bradley, R., "Inverse Simulation as a Tool for Flight Dynamics Research – Principles and applications", *Progress in Aerospace Sciences*, Vol. 42, 2006, pp. 174–210.

[9] Thomson, D.G., and Bradley, R., "Recent Developments in the Calculation of Inverse Solutions of the Helicopter Equations of Motion," Proceedings of the UK simulation Council Triennial Conference, September 1987.

[10] Thomson, D.G., and Bradley, R., "Development and Verification of an Algorithm for Helicopter Inverse Simulation," *Vertica*, Vol. 14, No. 2, 1990, pp. 185–200.

[11] Hess, R.A., Gao, C., and Wang, S.H., "Generalized Technique for Inverse Simulation Applied to Aircraft Maneuvers," *Journal of Guidance, Control, and Dynamics*, Vol. 14, (5), September–October 1991, pp. 920–926.

[12] Hess, R.A., Gao, C., "A Generalized Algorithm for Inverse Simulation Applied to Helicopter Maneuvering Flight," *Journal of the American Helicopter Society*, Vol. 38, No. 3, October 1993, pp. 3–15.

[13] Rutherford, S., and Thomson, D.G., "Improved Methodology for Inverse Simulation," *The Aeronautical Journal*, Vol. 100, No. 993, March 1996, pp. 79–86.

[14] de Matteis, G., de Socio, L.M., and Leonessa, A., "Solution of Aircraft Inverse Problems by Local Optimization," *Journal of Guidance, Control, and Dynamics*, Vol. 18, No. 3, May-June 1995, pp. 567–571.

[15] Celi, R., "Optimization-based inverse simulation of a Helicopter Slalom Maneuver," Proceedings of the 25th European Rotorcraft Forum, Rome, Italy, 1999.

[16] Rajmohan, N., Manivannan, V., Sankar, L.N., Costello. M.,"Development of a Methodology for Coupling Rotorcraft Aeromechanics and Vehicle Dynamics to study Helicopters in Maneuvering Flight," American Helicopter Society 65th Annual Forum Proceedings, Dallas, TX, May 27–29, 2009.

[17] Rajmohan, N., Manivannan, V., Sankar, L.N., Costello. M., "Effect of Inflow Modeling on Coupling between Rotor Flight Mechanics and Aeromechanics," 49th AIAA Aerospace Sciences Meeting including the New Horizons Forum and Aerospace Exposition, Orlando, FL, January 4–7, 2011.

[18] Abhishek, A., and Prasad, R., "Helicopter Unsteady Maneuver Analysis Using Inverse Flight Dynamics Simulation and Comprehensive Analysis," *Journal of Aircraft*, Article in Advance,DOI: 10.2514/1.C033707

[19] Abhishek, A., Datta, A., and Chopra, I.,"Prediction of UH-60A Structural Loads Using Multibody Analysis and Swashplate Dynamics," *Journal of Aircraft*, Vol. 46, No. 2, 2009, pp. 474–490.

[20] Davis, S.J., "Predesign Study for a Modern 4-Bladed Rotor for the RSRA," NASA CR-166155, March 1981.

[21] Bousman, W.G., "Aerodynamic Characteristics of SC1095 and SC1094 R8 Airfoils," NASA TP-2003-212265, December 2003.

[22] Howlett, J.J., "UH-60A Black Hawk Engineering Simulation Program," NASA CR 166309, December 1981.

[23] Kufeld, R.M., Balough, D.L., Cross, J.L., Studebaker, K.F., Jennison, C. D., and Bousman, W. G., "Flight Testing of the UH-60A Airloads Aircraft," American Helicopter Society 50th Annual Forum Proceedings, Washington, D. C., May 1994.

[24] Pitt, D.M., and Peters, D.A., "Rotor Dynamic Inflow Derivatives and Time Constants from Various Inflow Models," Proceedings of the 9th European Rotorcraft Forum, Stressa, Italy, September 1983.

[25] Houbolt,J.C., Brooks, G.W., "Differential Equations of Motion for Combined Flapwise Bending, Chordwise Bending and Torsion of Twisted, Nonuniform Rotor Blades," NASA Report 1346, 1958.

[26] Leishman, J.G., and Nguyen, K.Q., "State-Space Representation of Unsteady Airfoil Behavior," *AIAA Journal*, Vol.28, No. 5, pp. 836–844.

[27] Leishman, J.G., and Beddoes, T.S., "A Generalized Model for Unsteady Aerodynamic Behavior and Dynamic Stall Using Indicial Method," *Journal of the American Helicopter Society*, Vol. 34, No. 3, 1989,pp. 3–17.

[28] Ananthan, S., and Leishman, J.G., "Predictions of Transient Rotor Wake Aerodynamics in Response to Time-Dependant Blade Pitch Inputs," *Journal of Aircraft*, Vol. 41, No. 5, 2004, pp. 1025–1041.